

Uniaxial  $c$ -axis pressure effects on the underdoped superconductor  $\text{BaFe}_2(\text{As}_{0.72}\text{P}_{0.28})_2$ Ding Hu<sup>1,2,\*</sup>, David W. Tam,<sup>2</sup> Wenliang Zhang,<sup>3</sup> Yuan Wei,<sup>3</sup> Robert Georgii,<sup>4</sup>  
Björn Pedersen,<sup>4</sup> Alfonso Chacon Roldan,<sup>5</sup> and Pengcheng Dai<sup>2,1,†</sup><sup>1</sup>Center for Advanced Quantum Studies and Department of Physics, Beijing Normal University, Beijing 100875, China<sup>2</sup>Department of Physics and Astronomy, Rice University, Houston, Texas 77005-1827, USA<sup>3</sup>Beijing National Laboratory for Condensed Matter Physics, Institute of Physics, Chinese Academy of Sciences, Beijing 100190, China<sup>4</sup>Heinz Maier-Leibnitz Zentrum, Technische Universität München, D-85748 Garching, Germany<sup>5</sup>Physik-Department, Technische Universität München, D-85748 Garching, Germany

(Received 27 December 2018; revised manuscript received 27 March 2019; published 28 January 2020)

The optimal superconductivity ( $T_c \approx 30$  K) in  $\text{BaFe}_2(\text{As}_{1-x}\text{P}_x)_2$  can be reached when the coupled antiferromagnetic (AF) order ( $T_N$ ) and orthorhombic lattice distortion ( $T_s$ ) are suppressed to zero temperature with increasing of P concentration or hydrostatic pressure. Here we use transport and neutron scattering to study the  $c$ -axis pressure effects on electronic phases in underdoped  $\text{BaFe}_2(\text{As}_{0.72}\text{P}_{0.28})_2$ , which has  $T_N = T_s \approx 40$  K and  $T_c \approx 28$  K at zero pressure. With increasing  $c$ -axis pressure,  $T_N$  and  $T_s$  are slightly enhanced around  $P_c \sim 20$  MPa. Upon further increasing pressure, AF order is gradually suppressed to zero, while  $T_c$  is enhanced to 30 K. Our results reveal the importance of magnetoelastic couplings in  $\text{BaFe}_2(\text{As}_{1-x}\text{P}_x)_2$ , suggesting that the  $c$ -axis pressure can be used as a tuning parameter to manipulate the electronic phases in iron pnictides.

DOI: [10.1103/PhysRevB.101.020507](https://doi.org/10.1103/PhysRevB.101.020507)

The parent compounds of iron-based superconductors are long-range ordered antiferromagnets below a Néel temperature  $T_N$  and also display tetragonal to orthorhombic lattice distortion below  $T_s$  ( $T_s \geq T_N$ ) [1–3]. High-temperature superconductivity in these materials can be induced by charge-carrier doping, chemical pressure, and hydrostatic pressures that act to suppress  $T_N$  and  $T_s$  in a manner akin to other unconventional superconductors such as cuprates and heavy fermions [4]. To understand the microscopic origin of superconductivity, it is therefore important to sort out the interplay amongst magnetism, lattice distortion, and superconductivity. Compared with charge-carrier doping and chemical pressure via element substitution, which can also cause lattice disorder, hydrostatic and uniaxial pressure can tune the electronic, magnetic, and superconducting properties of the system without inducing additional lattice disorder [5–15].

$\text{BaFe}_2\text{As}_2$ , one of the parent compounds of iron-based superconductors, undergoes a tetragonal to orthorhombic structural transition at  $T_s$  and orders in a collinear antiferromagnetic (AF) structure below  $T_N$  ( $T_N \approx T_s \approx 140$  K) [16,17]. Upon electron or hole doping to form  $\text{BaFe}_{2-x}T_x\text{As}_2$  ( $T = \text{Co}, \text{Ni}$ ) [18–20] or  $\text{Ba}_{1-x}A_x\text{Fe}_2\text{As}_2$  ( $A = \text{K}, \text{Na}$ ) [21,22], static AF order is suppressed and exotic magnetic phases such as incommensurate and  $C_4$  magnetic order appear before doping-induced optimal superconductivity. In the case of isoelectronic doped  $\text{BaFe}_2(\text{As}_{1-x}\text{P}_x)_2$ , the structural and AF phase transitions are always coupled and increasing P doping suppresses  $T_s/T_N$  near  $x = 0.30$  where the optimal superconductivity is achieved at  $T_c \approx 30$  K [23,24]. The substitution on the arsenic site by the smaller phosphorous atom is regarded

as introducing chemical pressure in the system. Magnetic susceptibility measurements under hydrostatic pressure of underdoped  $\text{BaFe}_2(\text{As}_{1-x}\text{P}_x)_2$  point to a similar superconducting phase diagram with maximum  $T_c \approx 30$  K [11,25]. Given the similar electronic phase diagrams of P-doped and hydrostatic pressured  $\text{BaFe}_2(\text{As}_{1-x}\text{P}_x)_2$ , it would be interesting to test the effect of uniaxial pressure of the electronic phase diagram of the system [25,26].

Previous study on  $\text{BaFe}_2(\text{As}_{1-x}\text{P}_x)_2$  with in-plane strain added along the orthorhombic axis reveals increased  $T_N$  and decreased  $T_c$ , suggesting that the effect of the in-plane strain is similar to decreasing  $x$  by shifting the phase diagram [27,28]. These results are analogous to the effect of an in-plane strain on electron-doped  $\text{BaFe}_{2-x}T_x\text{As}_2$  ( $T = \text{Co}, \text{Ni}$ ) [14,29]. Since in-plane strain already breaks the  $C_4$  symmetry of the tetragonal phase and induces orthorhombic lattice distortion, strain-induced AF order reveals the subtle balance between magnetism and superconductivity. On the other hand, pressure dependence of the thermodynamic measurements reveal that a  $c$ -axis aligned uniaxial strain on  $\text{BaFe}_2(\text{As}_{1-x}\text{P}_x)_2$  increases  $T_c$  and may correspond to an increased P-doped level [28]. Therefore, it is surprising that our recent neutron diffraction and transport measurements on optimally doped  $\text{BaFe}_2(\text{As}_{0.70}\text{P}_{0.30})_2$  found that a  $c$ -axis aligned uniaxial pressure can spontaneously induce static stripe AF order with slightly suppressed  $T_c$  [30].

As the AF order and nematic phase in  $\text{BaFe}_2(\text{As}_{1-x}\text{P}_x)_2$  disappear in a weakly first-order fashion near optimal superconductivity [Fig. 1(a)], the  $T_N/T_s$  is sensitive to change of phosphorous concentration near  $x = 0.30$  [24]. Thus, we choose to carry out transport and neutron-diffraction studies on the underdoped compound  $\text{BaFe}_2(\text{As}_{0.72}\text{P}_{0.28})_2$  with  $T_N = T_s \approx 40$  K and  $T_c \approx 28$  K, to further investigate the effect of a  $c$ -axis pressure on the electronic properties of

\*dinghuphys@gmail.com

†pdai@rice.edu

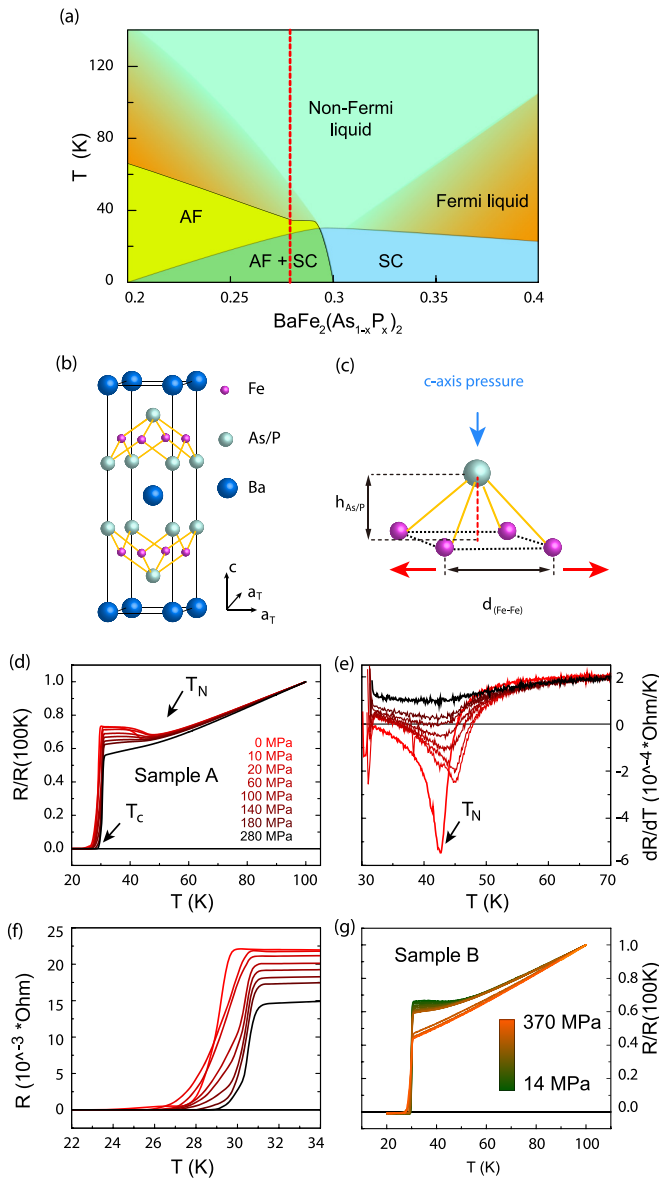


FIG. 1. (a) The schematic electronic phase diagram of  $\text{BaFe}_2(\text{As}_{1-x}\text{P}_x)_2$  with  $0.2 < x < 0.4$  [31], where antiferromagnetic order (AF), superconductivity (SC), Fermi liquid, and non-Fermi liquid are marked. The red dashed line marks the position of the  $x = 0.28$  compound measured in this work. (b) The crystal structure of  $\text{BaFe}_2(\text{As}_{1-x}\text{P}_x)_2$ . The purple, silver, and blue balls indicate the Fe, As/P, and Ba positions, respectively. (c) The schematic diagram of the FeAs tetrahedron. The red arrow indicates the increasing Fe-Fe distance due to a  $c$ -axis pressure. (d) Temperature dependence of the in-plane resistance for pressures up to 280 MPa along the  $c$  axis below 100 K of sample A. Data were normalized to 100 K resistance. (e) The temperature derivative of the in-plane resistance at different pressure of sample A, which reveals the  $T_N$  and  $T_S$  more clearly. (f) Temperature dependence of the resistance around 30 K at different pressures of sample A reveal the superconducting transition temperature evolution. (g) Temperature dependence of resistance under  $c$ -axis pressures of sample B, which is another single crystal from the same batch of sample A.

$\text{BaFe}_2(\text{As}_{1-x}\text{P}_x)_2$  and determine the origin of the observed quantum critical fluctuation near optimal superconductivity

[24,31–33]. We find that a  $c$ -axis aligned uniaxial pressure can significantly affect the AF ordering temperature  $T_N$ , while only slightly modifying the superconducting transition temperature  $T_c$ . As a function of increasing uniaxial pressure  $P_c$ ,  $T_N$  and  $T_S$  are first slightly enhanced at  $P_c \sim 20$  MPa. Then, they are gradually suppressed to zero at  $P_c \sim 280$  MPa with  $T_c \approx 30$  K. These results suggest that a  $c$ -axis aligned pressure can be used as a tuning parameter to manipulate the complex electronic phases in iron pnictides.

We chose to study the effects of a  $c$ -axis aligned uniaxial pressure on the slightly underdoped  $\text{BaFe}_2(\text{As}_{0.72}\text{P}_{0.28})_2$  superconductor with  $T_N = T_S \approx 40$  K and  $T_c \approx 28$  K, because of its close proximity to optimal superconductivity but with distinctively different electronic phases to the  $x = 0.30$  compound in zero pressure [24]. The crystal structure of  $\text{BaFe}_2(\text{As}_{1-x}\text{P}_x)_2$  and its response to a  $c$ -axis aligned pressure is shown in Figs. 1(b) and 1(c) [30]. A custom-designed pneumatic uniaxial pressure apparatus was used in the transport measurements, which can control the applied pressure precisely regardless of thermal contraction of the sample and apparatus [14,30]. The  $c$ -axis pressures have been applied successively at 300 K on the same  $\text{BaFe}_2(\text{As}_{0.72}\text{P}_{0.28})_2$  crystal in each measurement.

Figure 1(d) shows the temperature dependence of the resistivity at different  $c$ -axis pressures up to 280 MPa on sample A. At zero pressure, we find a kink around 40 K due to the AF order and orthorhombic structure transition [24]. With increasing  $P_c$ , the superconducting transition temperature gradually increases and reaches maximum ( $T_c \approx 30$  K) with the disappearance of the kink above  $T_c$  at  $P_c = 280$  MPa.

Assuming that the kink in temperature dependence of the resistivity indeed arises from AF order, we can determine  $c$ -axis pressure evolution of the ordering transition  $T_N$  by plotting the resistivity derivative  $dR/dT$  versus  $P_c$  in Fig. 1(e). Inspection of the figure reveals only one clear dip at each pressure, similar to the results measured in ambient conditions and in-plane strain on  $\text{BaFe}_2(\text{As}_{1-x}\text{P}_x)_2$  compounds [24,27,28], suggesting coupled AF order and orthorhombic lattice distortion at all studied pressures. This is different from the electron-doped pnictides where two anomalies in  $dR/dT$  correspond to the distinct  $T_S$  and  $T_N$ , respectively [34].

As a function of increasing  $P_c$ ,  $T_N$  shown as a dip in  $dR/dT$  increases slightly below 20 MPa, then it gradually decreases until vanishing at  $P_c = 280$  MPa. Figure 1(f) shows the temperature dependence of the resistivity near  $T_c$  as a function of  $P_c$ . With increasing  $P_c$ , we see a slight increase in  $T_c$  until the maximum  $T_c \approx 30$  K is achieved around 280 MPa. We note that the normal state resistance behavior above  $T_N$  at low pressures is different from the curve of 280 MPa. To confirm these results, we carried out the resistance measurements on another single crystal from the same batch marked as sample B. Similar to sample A, we find that uniaxial pressure indeed suppresses the AF order continuously, until it vanishes around 300 MPa [Fig. 1(g)].

The reduction in  $T_N$  and the increased  $T_c$  for  $20 \text{ MPa} < P_c < 280 \text{ MPa}$  is also seen in previous work where the value of  $P_c$  is unknown [28].

To confirm the pressure-induced changes in AF order, we carried out neutron-diffraction experiments in the same compound using the MIRA triple-axis spectrometer at

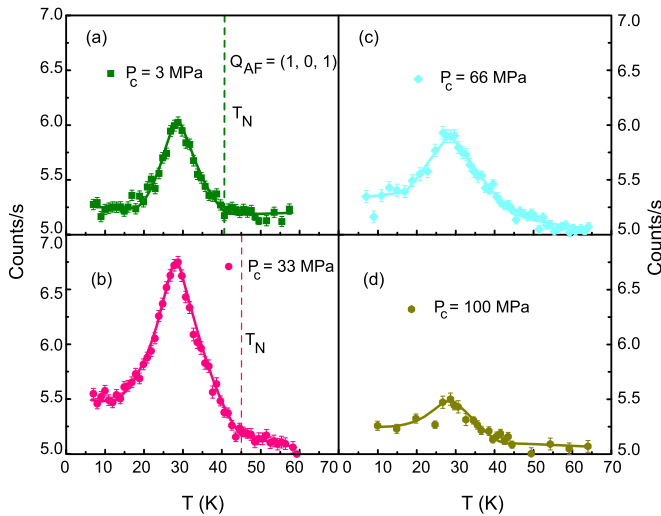


FIG. 2. Temperature dependence of the magnetic scattering intensity measured on MIRA-II for  $\text{BaFe}_2(\text{As}_{0.72}\text{P}_{0.28})_2$  with a *c*-axis pressure of (a)  $P_c = 3$  MPa, (b) 33 MPa, (c) 66 MPa, and (d) 100 MPa at  $\mathbf{Q}_{AF} = (1, 0, 1)$ . The solid lines are guides to the eye. Four figures are plotted in the same vertical scale so pressure-induced magnetic scattering change can be directly compared. Dashed lines in (a) and (b) mark the AF transition temperatures  $T_N$ .

Maier-Leibnitz Zentrum (MLZ), Garching, Germany [35,36]. The  $\text{BaFe}_2(\text{As}_{0.72}\text{P}_{0.28})_2$  crystal was clamped between two Al plates and loaded in an *in situ* uniaxial pressure cell [37]. Due to the large single crystal used to ensure the signal strength in neutron scattering experiments, the *in situ* uniaxial pressure cell cannot reach the high pressure limit of the transport measurements as shown in Fig. 1(d).

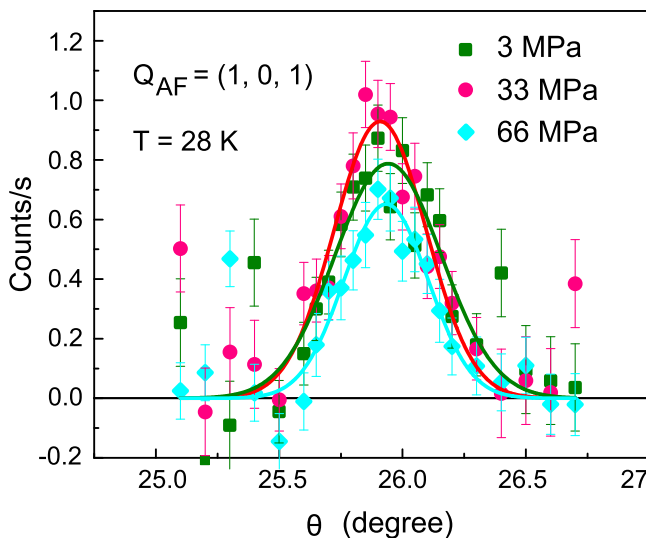


FIG. 3. Rocking scans across the  $\mathbf{Q}_{AF} = (1, 0, 1)$  position measured under different pressures. The solid lines are Gaussian fits to the data. The signals are measured at 28 K with background subtracted. The background scattering is measured above  $T_N$  but at different temperatures, it may result in intensity comparison of the pressure dependence of the scattering to be different from those of Fig. 2.

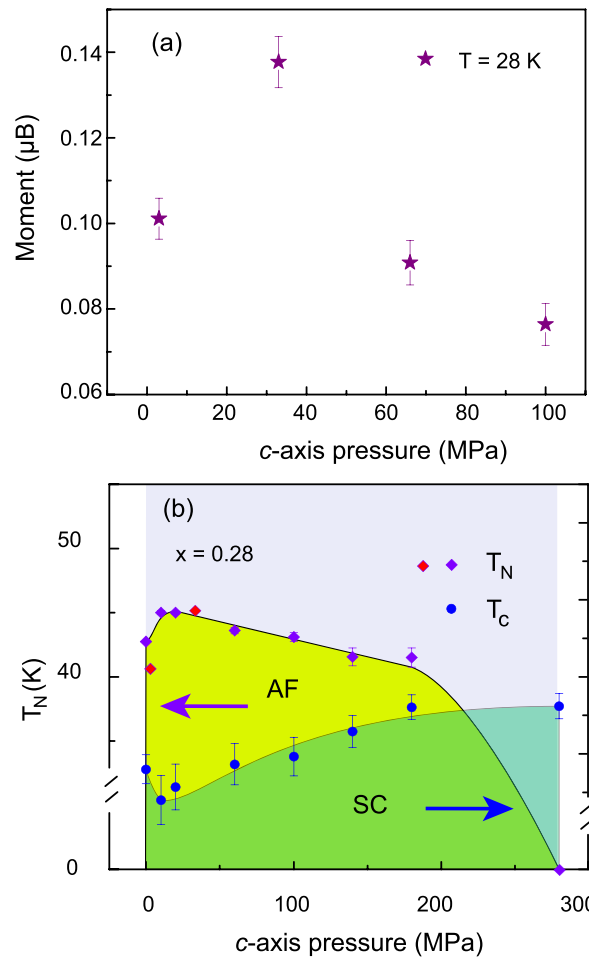


FIG. 4. (a) The *c*-axis pressure dependence of the ordered magnetic moment at  $T = 28$  K estimated assuming a stripe AF structure. The ordered moments are calculated from comparing the magnetic signal intensity from the temperature scans with a weak nuclear structure peak intensity. (b) Electronic phase diagram of  $\text{BaFe}_2(\text{As}_{0.72}\text{P}_{0.28})_2$  as a function of *c*-axis applied pressure extracted from the transport data of Fig. 1. The diamonds and circles are  $T_N$ 's and  $T_C$ 's corresponding to the left and right scales, respectively. Red diamonds are  $T_N$ 's obtained from the neutron data.

Figure 2 summarizes temperature dependence of the scattering at the AF ordering wave vector  $\mathbf{Q}_{AF} = (1, 0, 1)$  for pressures up to 100 MPa. At  $P_c \approx 3$  MPa, the  $\text{BaFe}_2(\text{As}_{0.72}\text{P}_{0.28})_2$  orders below 40 K [Fig. 2(a)]. The reduction in magnetic scattering below  $\approx 28$  K is due to the appearance of superconductivity [30]. Upon application of a  $P_c \approx 33$  MPa pressure, the  $T_N$  increases from  $\approx 40$  K to  $\approx 44$  K. Although it is difficult to determine the  $T_N$  precisely from the temperature dependence of the magnetic scattering at 66 and 100 MPa, we can clearly see the reduction in magnetic scattering with increasing pressure. Benefiting from the *in situ* pressure cell used in the measurements, we can compare the scattering intensity in Figs. 2(a)–2(d) directly and estimate the magnetic ordered moment at 28 K assuming a stripe AF structure. The magnetic ordered moment reaches a maximum at 33 MPa and then decreases with further increasing pressure [Figs. 3 and 4(a)], consistent with the evolution of  $T_N$

determined from transport measurements in Fig. 1. Figure 3 shows the rocking scans through the  $Q_{AF}$  AF Bragg peak at 28 K, indicating that uniaxial pressure does not change magnetic correlation length. These results confirm that the pressure evolution of resistivity data is due to bulk property changes in the system and consistent with a nonmonotonic suppression of the magnetic order before it vanishes at 280 MPa.

To summarize the transport and neutron scattering results, we plot in Fig. 4(b) the magnetic ( $T_N$ ) and superconducting ( $T_c$ ) transition temperatures as a function of  $P_c$ . Both  $T_N$  and  $T_c$  in Fig. 4(b) are determined from the  $dR/dT$  curves of transport data shown in Fig. 1. The  $T_N$ 's determined from our neutron-diffraction experiments in Figs. 2(a) and 2(b) have also been plotted, and their differences to the transport measurements can be attributed to the accuracy of neutron measurements and/or tiny differences in phosphorous concentrations between the two crystals used in these measurements. With increasing pressure,  $T_N$  approximately decreases continuously for  $P_c > 20$  MPa before vanishing abruptly at  $P_c = 280$  MPa where optimal superconductivity with  $T_c \approx 30$  K is achieved. Simple linear fits to the data for  $20 \text{ MPa} < P_c < 280 \text{ MPa}$  yield a reduction in  $T_N$  of  $-25 \pm 3 \text{ K/GPa}$ . For comparison, we note that for optimal  $x = 0.30$  compound, a  $c$ -axis pressure can induce a  $T_N$  increase at the rate of  $48 \pm 2 \text{ K/GPa}$  [30], suggesting the sensitivity of magnetism to quantum fluctuations near optimal superconductivity in  $\text{BaFe}_2(\text{As}_{1-x}\text{P}_x)_2$ . Although neutron-diffraction measurements in the high-pressure regime of  $P_c > 100$  MPa is desirable to confirm the suppression of  $T_N$  to zero attributed from the disappearance of the dip in  $dR/dT$  in transport measurements, such experiments are rather difficult for the *in situ* uniaxial pressure device used in the neutron-diffraction experiments.

In general, electronic phases in iron pnictides such as  $\text{BaFe}_2(\text{As}_{1-x}\text{P}_x)_2$  are believed to be related with crystal

structural parameters including pnictogen height (the height of As/P to the Fe layer),  $a$ ,  $c$ , and the  $c/a$  ratio [38–41]. Specifically, increasing the P-doping level in  $\text{BaFe}_2(\text{As}_{1-x}\text{P}_x)_2$  is linearly associated with decreasing pnictogen height,  $a$  and  $c$  axis, while the  $c/a$  is held constant [42]. For comparison, a  $c$ -axis pressure, while it decreases the  $c$ -axis and expands  $a$ -axis lattice constants, barely changes the iron-pnictogen height [30]. From the  $P_c$  dependence of the electronic phase diagram in Fig. 4(b), we see the nonmonotonic evolution of the AF order in  $\text{BaFe}_2(\text{As}_{0.72}\text{P}_{0.28})_2$  before its disappearance around  $P_c \approx 280$  MPa with the appearance of optimal superconductivity. Although a microscopic origin of such a phase diagram is still unclear, our results suggest that both the out-of-plane and in-plane magnetoelastic coupling are important for optimal superconductivity and the appearance of a quantum critical point.

In summary, we have systematically studied the  $c$ -axis uniaxial pressure evolution of the AF phase and superconductivity in the underdoped  $\text{BaFe}_2(\text{As}_{0.72}\text{P}_{0.28})_2$  superconductor. With increasing  $P_c$ , the AF order can be gradually suppressed to zero at around  $P_c = 280$  MPa with the appearance of optimal superconductivity, after the initial enhancement at  $\sim 20$  MPa. These results indicate that in addition to iso-electronic doping and hydrostatic pressure, uniaxial pressure along the  $c$  axis can be used as a tuning parameter to manipulate the electronic phases and study in the interplay of magnetism and superconductivity in iron pnictides.

The work at Beijing Normal University is supported by the Fundamental Research Funds for the Central Universities (Grants No. 310432101 and No. 2014JJC27). The neutron scattering work at Rice is supported by US NSF Grant No. DMR-1700081 (P.D.). A part of the material synthesis work at Rice is supported by Robert A. Welch Foundation Grant No. C-1839 (P.D.).

- 
- [1] Y. Kamihara, T. Watanabe, M. Hirano, and H. Hosono, *J. Am. Chem. Soc.* **130**, 3296 (2008).
- [2] G. R. Stewart, *Rev. Mod. Phys.* **83**, 1589 (2011).
- [3] P. C. Dai, *Rev. Mod. Phys.* **87**, 855 (2015).
- [4] D. J. Scalapino, *Rev. Mod. Phys.* **84**, 1383 (2012).
- [5] L. Sun, X. J. Chen, J. Guo, P. Gao, Q. Z. Huang, H. Wang, M. Fang, X. Chen, G. Chen, Q. Wu, C. Zhang, D. Gu, X. Dong, L. Wang, K. Yang, A. Li, X. Dai, H. K. Mao, and Z. Zhao, *Nature (London)* **483**, 67 (2012).
- [6] M. S. Torikachvili, S. L. Bud'ko, N. Ni, and P. C. Canfield, *Phys. Rev. Lett.* **101**, 057006 (2008).
- [7] H. Takahashi, K. Igawa, K. Arii, Y. Kamihara, M. Hirano, and H. Hosono, *Nature (London)* **453**, 376 (2008).
- [8] S. Medvedev, T. M. McQueen, I. A. Troyan, T. Palasyuk, M. I. Erements, R. J. Cava, S. Naghavi, F. Casper, V. Ksenofontov, G. Wortmann, and C. Felser, *Nat. Mater.* **8**, 630 (2009).
- [9] M. Tomić, R. Valentí, and H. O. Jeschke, *Phys. Rev. B* **85**, 094105 (2012).
- [10] T. Yamazaki, N. Takeshita, R. Kobayashi, H. Fukazawa, Y. Kohori, K. Kihou, C.-H. Lee, H. Kito, A. Iyo, and H. Eisaki, *Phys. Rev. B* **81**, 224511 (2010).
- [11] W. J. Duncan, O. P. Welzel, C. Harrison, X. F. Wang, X. H. Chen, F. M. Grosche, and P. G. Niklowitz, *J. Phys.: Condens. Matter* **22**, 052201 (2010).
- [12] C. Dhital, Z. Yamani, W. Tian, J. Zeretsky, A. S. Sefat, Z. Wang, R. J. Birgeneau, and S. D. Wilson, *Phys. Rev. Lett.* **108**, 087001 (2012).
- [13] X. Lu, J. T. Park, R. Zhang, H. Luo, A. H. Nevidomskyy, Q. Si, and P. Dai, *Science* **345**, 657 (2014).
- [14] D. W. Tam, Y. Song, H. R. Man, S. C. Cheung, Z. P. Yin, X. Y. Lu, W. Y. Wang, B. A. Frandsen, L. Liu, Z. Z. Gong, T. U. Ito, Y. P. Cai, M. N. Wilson, S. L. Guo, K. Koshiishi, W. Tian, B. Hitti, A. Ivanov, Y. Zhao, J. W. Lynn, G. M. Luke, T. Berlijn, T. A. Maier, Y. J. Uemura, and P. C. Dai, *Phys. Rev. B* **95**, 060505(R) (2017).
- [15] H. R. Man, R. Zhang, J. T. Park, X. Y. Lu, J. Kulda, A. Ivanov, and P. C. Dai, *Phys. Rev. B* **97**, 060507(R) (2018).

- [16] Q. Huang, Y. Qiu, W. Bao, M. A. Green, J. W. Lynn, Y. C. Gasparovic, T. Wu, G. Wu, and X. H. Chen, *Phys. Rev. Lett.* **101**, 257003 (2008).
- [17] M. G. Kim, D. K. Pratt, G. E. Rustan, W. Tian, J. L. Zarestky, A. Thaler, S. L. Bud'ko, P. C. Canfield, R. J. McQueeney, A. Kreyssig, and A. I. Goldman, *Phys. Rev. B* **83**, 054514 (2011).
- [18] H. Luo, R. Zhang, M. Laver, Z. Yamani, M. Wang, X. Lu, M. Wang, Y. Chen, S. Li, S. Chang, J. W. Lynn, and P. Dai, *Phys. Rev. Lett.* **108**, 247002 (2012).
- [19] X. Lu, H. Gretarsson, R. Zhang, X. Liu, H. Luo, W. Tian, M. Laver, Z. Yamani, Y.-J. Kim, A. H. Nevidomskyy, Q. Si, and P. Dai, *Phys. Rev. Lett.* **110**, 257001 (2013).
- [20] D. K. Pratt, M. G. Kim, A. Kreyssig, Y. B. Lee, G. S. Tucker, A. Thaler, W. Tian, J. L. Zarestky, S. L. Bud'ko, P. C. Canfield, B. N. Harmon, A. I. Goldman, and R. J. McQueeney, *Phys. Rev. Lett.* **106**, 257001 (2011).
- [21] S. Avci, O. Chmaissem, J. M. Allred, S. Rosenkranz, I. Eremin, A. V. Chubukov, D. E. Bugaris, D. Y. Chung, M. G. Kanatzidis, J.-P. Castellan, J. A. Schlueter, H. Claus, D. D. Khalyavin, P. Manuel, A. Daoud-Aladine, and R. Osborn, *Nat. Commun.* **5**, 3845 (2014).
- [22] A. E. Böhmer, F. Hardy, L. Wang, T. Wolf, P. Schweiss, and C. Meingast, *Nat. Commun.* **6**, 7911 (2015).
- [23] J. M. Allred, K. M. Taddei, D. E. Bugaris, S. Avci, D. Y. Chung, H. Claus, C. dela Cruz, M. G. Kanatzidis, S. Rosenkranz, R. Osborn, and O. Chmaissem, *Phys. Rev. B* **90**, 104513 (2014).
- [24] D. Hu, X. Y. Lu, W. L. Zhang, H. Q. Luo, S. L. Li, P. P. Wang, G. F. Chen, F. Han, S. R. Banjara, A. Sapkota, A. Kreyssig, A. I. Goldman, Z. Yamani, C. Niedermayer, M. Skoulatos, R. Georgii, T. Keller, P. S. Wang, W. Q. Yu, and P. C. Dai, *Phys. Rev. Lett.* **114**, 157002 (2015).
- [25] L. E. Klintberg, S. K. Goh, S. Kasahara, Y. Nakai, K. Ishida, M. Sutherland, T. Shibauchi, Y. Matsuda, and T. Terashima, *J. Phys. Soc. Jpn.* **79**, 123706 (2010).
- [26] H. Shishido, A. F. Bangura, A. I. Coldea, S. Tonegawa, K. Hashimoto, S. Kasahara, P. M. C. Rourke, H. Ikeda, T. Terashima, R. Settai, Y. Ōnuki, D. Vignolles, C. Proust, B. Vignolle, A. McCollam, Y. Matsuda, T. Shibauchi, and A. Carrington, *Phys. Rev. Lett.* **104**, 057008 (2010).
- [27] H.-H. Kuo, J. G. Analytis, J.-H. Chu, R. M. Fernandes, J. Schmalian, and I. R. Fisher, *Phys. Rev. B* **86**, 134507 (2012).
- [28] A. E. Böhmer, P. Burger, F. Hardy, T. Wolf, P. Schweiss, R. Fromknecht, H. v. Löhneysen, C. Meingast, H. K. Mak, R. Lortz, S. Kasahara, T. Terashima, T. Shibauchi, and Y. Matsuda, *Phys. Rev. B* **86**, 094521 (2012).
- [29] X. Lu, K.-F. Tseng, T. Keller, W. Zhang, D. Hu, Y. Song, H. Man, J. T. Park, H. Luo, S. Li, A. H. Nevidomskyy, and P. Dai, *Phys. Rev. B* **93**, 134519 (2016).
- [30] D. Hu, W. Wang, W. Zhang, Y. Wei, D. Gong, D. W. Tam, P. Zhou, Y. Li, G. Tan, Y. Song, R. Georgii, B. Pedersen, H. Cao, W. Tian, B. Roessli, Z. Yin, and P. Dai, *npj Quantum Mater.* **3**, 47 (2018).
- [31] T. Shibauchi, A. Carrington, and Y. Matsuda, *Annu. Rev. Condens. Matter Phys.* **5**, 113 (2014).
- [32] J. G. Analytis, H. H. Kuo, R. D. McDonald, M. Wartenbe, P. M. C. Rourke, N. E. Hussey, and I. R. Fisher, *Nat. Phys.* **10**, 197 (2014).
- [33] H. H. Kuo, J. H. Chu, J. C. Palmstrom, S. A. Kivelson, and I. R. Fisher, *Science* **352**, 958 (2016).
- [34] R. Zhang, D. Gong, X. Lu, S. Li, P. Dai, and H. Luo, *Supercond. Sci. Technol.* **27**, 115003 (2014).
- [35] R. Georgii and K. Seemann, *JLSRF* **1**, A3 (2015).
- [36] R. Georgii, T. Weber, G. Brandl, M. Skoulatos, M. Janoschek, S. Mühlbauer, C. Pfleiderer, and P. Böni, *Nucl. Instrum. Methods Phys. Res., Sect. A* **881**, 60 (2018).
- [37] A. Chacon, A. Bauer, T. Adams, F. Rucker, G. Brandl, R. Georgii, M. Garst, and C. Pfleiderer, *Phys. Rev. Lett.* **115**, 267202 (2015).
- [38] A. E. Böhmer, A. Sapkota, A. Kreyssig, S. L. Bud'ko, G. Drachuck, S. M. Saunders, A. I. Goldman, and P. C. Canfield, *Phys. Rev. Lett.* **118**, 107002 (2017).
- [39] D. C. Johnston, *Adv. Phys.* **59**, 803 (2010).
- [40] C. H. Lee, K. Kihoua, A. Iyo, H. Kito, P. M. Shirage, and H. Eisaki, *Solid State Commun.* **152**, 644 (2012).
- [41] Z. P. Yin, K. Haule, and G. Kotliar, *Nat. Phys.* **7**, 294 (2011).
- [42] S. Kasahara, T. Shibauchi, K. Hashimoto, K. Ikada, S. Tonegawa, R. Okazaki, H. Shishido, H. Ikeda, H. Takeya, K. Hirata, T. Terashima, and Y. Matsuda, *Phys. Rev. B* **81**, 184519 (2010).